1 Introduction

The performance of magnetic nanostructures is determined by their precisely engineered design and material properties. Therefore, their detailed inspection is indispensable prior to sensitive applications in many fields that range from local drug delivery or hyperthermia tumor treatment [Pan03] to high-density information storage [Ter05]. One focus of this work lies on establishing a novel x-ray method based on conventionally surface-sensitive photoemission electron microscopy that allows for the element-specific magnetic imaging of composite nanostructures as well as for the separate imaging of surface and bulk contributions [Kim11]. In particular in the field of magnetic data storage, industrial progress and underlying research have been exceptionally close ever since. Reaching fundamental limits such as superparamagnetism of down-scaled bits and unaddressability of non-perfect self-organized structures demands completely new concepts. In this respect, the so-called racetrack memory was proposed [Par05, Par08]. This non-volatile shift register is based on the effect that domain walls can be displaced by spin-polarized currents [Ber84, Klä03a, Tho07]. Franken *et al.* recently demonstrated a comparable concept based on field-driven domain-wall motion [Fra12c]. The precondition for the realization of such shift registers is to understand and control the pinning and the simultaneous propagation of domain walls in a periodic potential. Other promising applications basing on domain-wall motion are logic devices [All05] and lab-on-chip devices where microbeads trapped in the stray-fields of domain walls are employed for the directed transportation of biomolecules and cells [Bry10, Rap12]. Systematic studies of field- and current-driven domain-wall dynamics are prerequisites for the realization of the above mentioned devices. These studies require the reliable preparation of domain walls. Since high current densities can change or destroy the structures investigated, weak pinning potentials allowing for the depinning of domain walls at low current densities are desirable. It is decisive for the preparation of a domain wall at such pinning sites, that the domain wall is injected into a wire at fields smaller than the field required to depin the domain wall from the respective pinning site.

The perspective of this work is to find reliable methods for the preparation of domain walls in two different kinds of ferromagnetic nanostructures, namely lithographically patterned wires of Co/Pt multilayers with perpendicular magnetic anisotropy and electrochemically synthesized nickel and nickel-iron wires. Both systems are among the most promising candidates for novel devices that are based on the propagation of domain walls. Furthermore, they can serve as model systems for fundamental studies.

Systems with high uniaxial out-of-plane anisotropy as Co/Pt multilayers are characterized by comparably small domain-wall widths. Thus, they allow for higher storage density compared to in-plane magnetized materials. It has been shown both theoretically [Tat04, Xia06] and experimentally [Bou08, Alv10] that the non-adiabatic spin transfer, an effect that increases with decreasing domain-wall width, contributes to the efficiency of current-driven domain-wall motion. Another advantage of systems with high perpendicular magnetic anisotropy is that one-dimensional models can be applied to analyze their domain walls, which exhibit nearly perfect Bloch or Néel spin structures [Bou11], whereas in soft-magnetic wires with a stray-field driven in-plane magnetization complex two-dimensional spin structures with intrinsic degrees of freedom occur [Hay06b]. The simple domain-wall structure is also the reason why for example Co/Pt layered structures with out-of-plane anisotropy are frequently used to investigate the intrinsic domain wall resistance [Has06, Azi06, Fra12b]. Furthermore, for Bloch walls in perpendicularly magnetized wires the domain-wall resistance is not masked by contributions of the anisotropic magnetoresistance as the magnetization is orthogonal to the current direction everywhere.

Anodization of aluminum templates allows for the creation of pores with modulated diameters [Lee06]. The pores can be covered by atomic-layer deposition or filled by electrochemical deposition to synthesize complex three-dimensional nanostructures replicating the variations of the pore diameter [Pit09, Cho10, Pit11]. The possibility of cheap mass production of uniform particles with diameters down to a about 20 nm and aspect ratios up to 1000 makes this synthesis approach highly attractive for technological applications. It has been predicted that domain walls in cylindrical nanowires can act as massless objects [Yan10]. This implies that there is no Walker breakdown restricting the domain-wall velocity, and accordingly no fundamental limit for the performance of devices that are based on the fast movement of domain walls. Another aspect that is of interest for such applications is that there exists no threshold current for the displacement of massless domain walls. Soft-magnetic cylindrical wires are often declared as model systems for numerical simulations and analytical calculations based on infinite cylinders [Aha97a]. The validity of this approach is critically discussed in this work.

This thesis is structured as follows: chapter 2 gives an overview of the underlying physics. Section 2.1 focuses on the fundamentals of ferromagnetism including domain-wall theory. Section 2.2 deals with the preparation, depinning, and motion of domain walls in ferromagnetic nanowires. Introductions to magnetoresistive effects and to the x-ray magnetic circular dichroism (XMCD) effect, which is the basis of magnetic imaging using polarized x rays, follow in Secs. 2.3 and 2.4. Chapters 3 through 6 are dedicated to cylindrical nanowires. Chapter 3 gives an introduction to micromagnetic simulations and presents some results to illustrate the influence different energies have on the magnetic behavior of nanostructures. The synthesis of cylindrical nanowires as well as the methods employed for their characterization,

namely magnetoresistance measurements, magnetic force microscopy, and photoemission electron microscopy, are presented in chapter 4. Section 4.4 includes publication [Kim11] dealing with photoemission electron microscopy of three-dimensional magnetization configurations in core-shell nanostructures. Chapter 5 covers the results on straight nickel wires which are analyzed on the basis of the analytical curling model and micromagnetic simulations. The feasibility of controlled domain-wall preparation in wires manipulated with a focused ion beam, in bent wires, and in wires with diameter modulations serving as tailored pinning sites is the subject matter of chapter 6. Experimental aspects and results on Co/Pt multilayer wires are presented in chapter 7 that includes publication [Kim13]. Additional details on the sample preparation and magnetic imaging by transmission x-ray microscopy are given in the Appendix Secs. B.3 and B.6, respectively. The work closes with a conclusion in chapter 8.

2 Fundamentals

In this work, magnetization reversal in two different kinds of ferromagnetic nanostructures, namely cylindrical nanowires and flat wires of Co/Pt multilayers, is studied. This chapter gives an overview of the underlying physics. The first section starts with the fundamentals of ferromagnetism and domain theory. Subsections 2.1.5 and 2.1.6 discuss the Stoner-Wohlfarth model of coherent rotation and the curling model, two models for the analytical treatment of magnetization reversal. The section closes with an introduction to micromagnetism, the basis for micromagnetic simulations. Section 2.2 deals with the preparation, depinning, and motion of domain walls in ferromagnetic nanowires. An introduction to spin-dependent transport and a phenomenological overview of magnetoresistive effects follows in Sec. 2.3. In Sec. 2.4 the x-ray magnetic circular dichroism (XMCD) effect, which is the basis of magnetic imaging using polarized x rays, is explained.

2.1 Ferromagnetism

Magnetism has been an active field of study for more than 2 500 years [Stö06]. Many theoretical and experimental approaches have generated a variety of definitions and concepts. Addressing all exciting aspects of the topic lies beyond the scope of this work. This section is limited to the basics and to the aspects directly related to this work: the microscopic origin of ferromagnetism, vector fields used for its description, as well as energy considerations and reversal modes regarding the formation of ferromagnetic patterns, so-called domains.

2.1.1 Origin of ferromagnetism

In a free atom, there are three origins of a magnetic moment: the spin of the electron, the orbital angular momentum of the electron with respect to the movement around the core, and changes of the orbital angular momentum induced by an external magnetic field [Spa11]. The latter leads to diamagnetism, while the other two aspects are the sources of paramagnetism. Some paramagnetic materials show a phase transition at the so-called Curie temperature. Below this temperature cooperative magnetic ordering appears, and the material is ferromagnetic. Classical magnetic dipole-dipole

interactions between adjacent ions are not strong enough to account for such a spontaneous magnetization, since ordering is easily destroyed by thermal fluctuations at temperatures above a few millikelvin [Kop07]. The orientation of the magnetic moments in a ferromagnet is a quantum-mechanical phenomenon [Blu01]. The basic interaction is the exchange interaction. The Hamiltonian considering the exchange energy between two fermionic particles with spins $\vec{S}_i$ and $\vec{S}_j$ is given by [Whi07]

$$\hat{H}_{\text{ex}} = -2J\vec{S}_i \cdot \vec{S}_j. \tag{2.1}$$

J is the coupling constant depending on the difference between the symmetric and the antisymmetric product state of the single-particle wavefunctions. This Hamiltonian is the basis of some fundamental models for the description of ferromagnetic behavior. The most popular of these models is the **Heisenberg model** where the interaction between the individual spins in a three-dimensional lattice is described by the Heisenberg Hamiltonian

$$\hat{H} = -\sum_{i \neq j} J_{ij}\vec{S}_i \cdot \vec{S}_j \tag{2.2}$$

with the exchange integral $J_{ij} = \int\int \psi_i(\vec{r}_1)\psi_j(\vec{r}_2)\frac{e^2}{4\pi\epsilon_0 r_{12}}\psi_i^*(\vec{r}_2)\psi_j^*(\vec{r}_1)d\vec{r}_1 d\vec{r}_2$ [Hei28]. ψ_{ij} are the single-particle wavefunctions, $\epsilon_0 \cong 8.854 \cdot 10^{-12}\frac{\text{As}}{\text{Vm}}$ is the permittivity of vacuum, and $e \cong 1.602 \cdot 10^{-19}$ C is the elementary charge.

If J is positive the system prefers parallel spin orientation and the material is ferromagnetic. For negative J antiparallel alignment is favored and the material shows an antiferromagnetic spin structure. Only in few materials the exchange interaction is strong enough to force an alignment of adjacent spins. If there is no overlap of the electron wave functions the Hamiltonian is zero and magnetic ordering cannot be explained by direct exchange interaction [Stö06]. Indirect exchange interaction can be mediated by a diamagnetic ion between two magnetic ions, e.g. manganese oxide, or via excited states, e.g. europium oxide [Mat61]. Another type of indirect exchange is the Ruderman-Kittel-Kasuya-Yoshida (RKKY) interaction [Rud54]. This long-range interaction is caused by the coupling of the magnetic moments of well-shielded, low lying shells to the conduction electrons. It shows an oscillatory behavior depending on the distance between two ions [Nol86]. The RKKY interaction is responsible for the coupling between magnetic layers, the basis of giant magnetoresistance (GMR).

In the $3d$ transition metals iron, cobalt, and nickel as well as in their alloys, the main exchange interaction is mediated by the conduction electrons. The origin of ferromagnetic order in such systems can be described by the **Stoner model of ferromagnetism**, which incorporates the exchange interaction into the itinerant electron model [Sto38]. The model considers the density of states $D(E)$ as consisting of two subbands $D_\uparrow(E)$ and $D_\downarrow(E)$ for electrons with spin up and spin down, respectively.

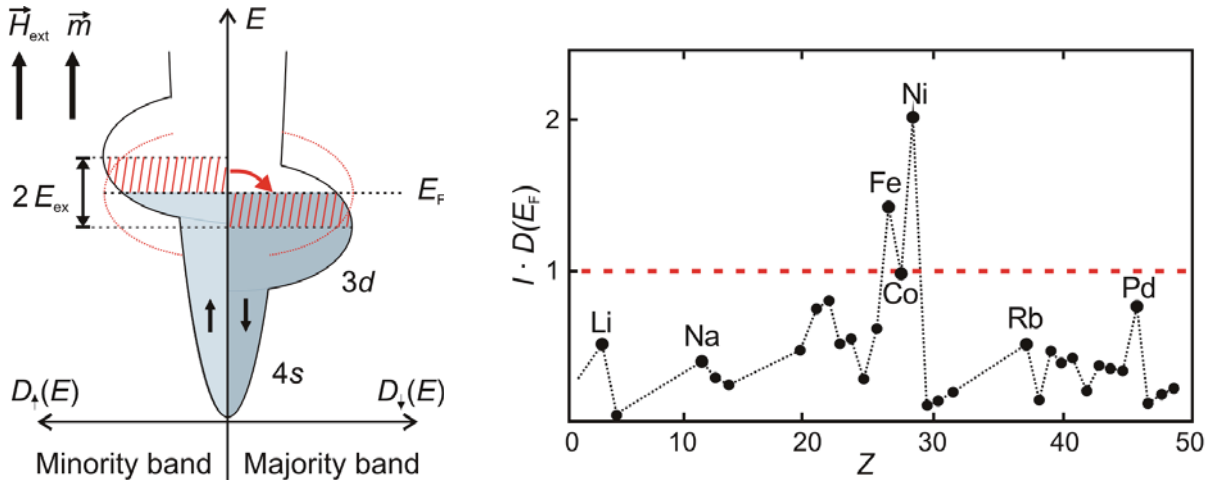

Figure 2.1: (a) Schematic of the spin-projected density of states of a $3d$ transition metal. Due to the exchange interaction the energy of the $3d$ electrons with a spin orientation antiparallel to the direction of an external field $\vec{H}_{\text{ext}}$ is lower by the exchange splitting $2\,E_{\text{ex}}$ what leads to a population change as indicated by the red shaded regions. The gray areas mark the resulting filled electron states below the Fermi energy E_{F}. The band with the larger amount of electrons with spin down is called 'majority band', while the other one is referred to as 'minority band' carrying the minority electrons. (b) Product of the density of states at the Fermi level $D(E_{\text{F}})$ and exchange integral I as a function of the atomic number Z. If the Stoner criterion $I \cdot D(E_{\text{F}}) \geq 1$ is fulfilled, a metal is ferromagnetic. After [Iba99].

In the presence of a magnetic field the degeneracy of electrons with opposite spin orientation is lifted and the two subbands get shifted by $\pm E_{\text{ex}}$. Electrons change from one subband to the other as indicated by the red shaded areas in Fig. 2.1(a). The increase in kinetic energy pays off by the energy reduction due to exchange interaction. The resulting difference in the number of electrons with spin up and spin down, also referred to as 'minority' and 'majority' electrons, leads to an effective magnetic moment $\vec{m}$. This magnetic moment is not necessarily an integer multiple of the Bohr magneton[1], as it is observed in iron (2.2 μ_{B}/atom), cobalt (1.7 μ_{B}/atom), and nickel (0.6 μ_{B}/atom)[O'H00]. The model predicts a ferromagnetic ordering if the **Stoner criterion**

$$I \cdot D(E_{\text{F}}) \geq 1 \tag{2.3}$$

is fulfilled [Sto38]. I is an exchange integral, and $D(E_{\text{F}})$ is the density of states at the Fermi level.

[1]The Bohr magneton is defined as $\mu_{\text{B}} = \frac{e\hbar}{2m_{\text{e}}} \cong 9.27 \cdot 10^{-24}\text{Am}^2$. $m_{\text{e}} \cong 9.109 \cdot 10^{-31}$ kg is the electron mass, $\hbar$ is Planck's constant divided by 2π.

In Fig. 2.1(b) the product $D(E_F) \cdot I$ is plotted for some materials. The $3d$ transition metals iron (Fe), cobalt (Co), and nickel (Ni) are ferromagnetic as predicted by the Stoner criterion. While I is element specific and not depending on the local environment, $D(E_F)$ is influenced by adjacent ions. Atoms at interfaces have less neighbors, i.e. the coordination number is decreased. As a consequence the $3d$ band carrying the magnetic moment gets narrower and tends to the bandstructure of a free atom [Bob04]. The bandwidth is inversely proportional to the density of states at the Fermi level. That is why more metals satisfy the Stoner criterion if surface effects come into play. Palladium (Pd) and platinum (Pt) for example can be ferromagnetic if they are prepared as thin films [Blü95].

2.1.2 Magnetic anisotropy

Anisotropy means that a physical property is a function of direction. The spontaneous magnetization of a ferromagnet is not oriented arbitrarily but aligned along preferential directions, the so-called easy axes (EA). Without this anisotropy magnetic order could hardly be observed, especially in two dimensional systems such as thin films [Bla94]. The reason for this is the short-range character of the exchange interaction. Magnetic anisotropy is usually caused by different contributions made up of surface and volume parts. The individual contributions are discussed below.

Surface and interface anisotropy originate from missing neighbors. At interfaces the overlap of the electron shells is reduced. This modifies the exchange energy and results in an anisotropic magnetization behavior [Cho69].

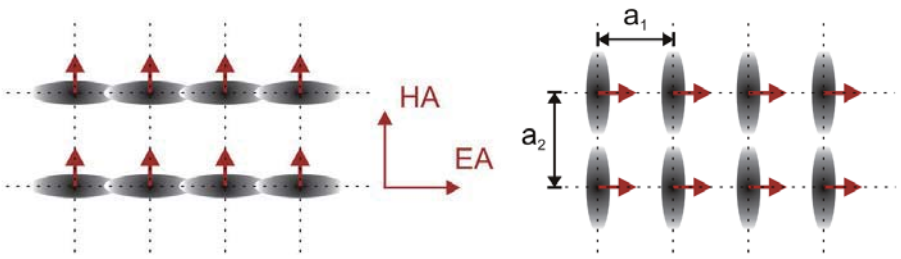

Figure 2.2: Microscopic origin of magnetocrystalline anisotropy. The gray shaded ellipses represent non-spherical charge distributions caused by spin-orbit interaction. In a cubic crystal with two different lattice constants a_1 and $a_2 > a_1$ the overlap of electron shells varies depending on the orientation of the associated magnetic moments indicated by the red arrows. For a hard axis (HA) magnetization the overlap is large (a), while for a magnetization along the easy axis (EA) the overlap and the concomitant exchange and electrostatic energy are reduced (b). After [Kit05].

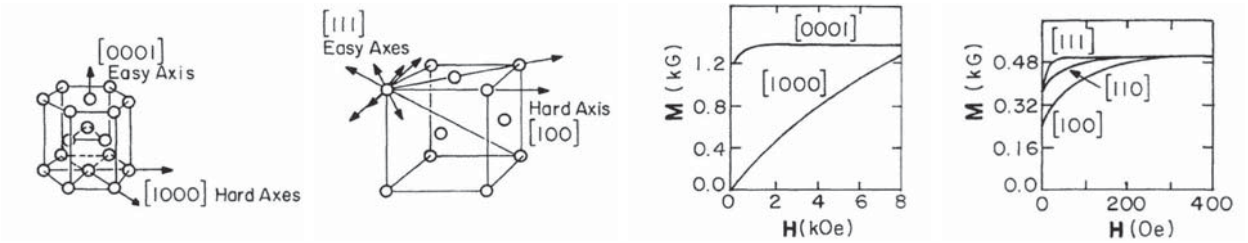

(a) (b) (c) (d)

Figure 2.3: (a) Hexagonal lattice structure of cobalt. (b) Face-centered cubic (fcc) structure of nickel. Magnetization versus field curves of (c) cobalt and (d) nickel for an external magnetic field H applied along different crystal axes. Reprinted with permission from [O'H00]. Copyright 2000 by John Wiley and Sons.

The volume anisotropy has several origins. **Magnetocrystalline anisotropy** reflects the symmetry of the crystal lattice [Kit49]. Its microscopic origin is illustrated in Fig. 2.2. The electron distribution of an atom is coupled to the spin direction. It is not always spherical but can be deformed by spin-orbit interaction. If in addition the crystal field seen by an atom is of low symmetry, an anisotropic interaction of the electron shells with the crystal field can be observed. Phenomenologically the magnetocrystalline anisotropy is defined as the largest difference of spin-orbit energy for a sample magnetized along two different directions. For strong spin-orbit interaction and anisotropic crystal fields as they are typical for rare-earth metals, the magnetocrystalline anisotropy is high [Bré07]. If the coupling of the orbital angular momentum to the lattice is stronger than the spin-orbit coupling, a rather weak magnetocrystalline anisotropy is observed. The latter is generally the case in $3d$ transition metals. Nevertheless, magnetocrystalline anisotropy can play a role in these materials, and shall be discussed for cobalt and nickel in the following.

Figure 2.3 shows the crystal structures of cobalt and nickel as well as their magnetization versus field curves[2] along different crystal axes. The hexagonal crystal structure of cobalt results in a uniaxial magnetocrystalline anisotropy with an easy axis along the c axis (<0001> direction). As revealed by the magnetization curves in Fig. 2.3(c) high external fields are required to align the magnetic moments of cobalt parallel to the basal plane. The magnetic field required to saturate the magnetization of a sample along a hard axis is called anisotropy field H_a. It is a quantitative measure for the strength of the magnetocrystalline anisotropy.

In systems with one preferred direction as cobalt or thin films with uniaxial magnetic anisotropy, the anisotropy energy density is given by [Hub09]

$$\epsilon_\mathrm{uniaxial} = K_\mathrm{u1} \sin^2\theta + K_\mathrm{u2} \sin^4\theta + ... \tag{2.4}$$

[2]Magnetization curves are discussed in more detail in the respective paragraph of Sec. 2.1.4.

where θ is the angle between the magnetization direction and the easy axis. K_{u1} and K_{u2} are the anisotropy constants. At room temperature only the lowest order terms of the energy densities have to be considered, since contributions of higher orders are averaged out by thermal excitations.

Nickel usually crystallizes in a face centered cubic (fcc) structure as shown in Fig. 2.3(b). Like iron and permalloy nickel has a cubic anisotropy which in bulk is described by the energy density

$$\epsilon_{\text{cubic}} = K_{c1}(\alpha_1^2\alpha_2^2 + \alpha_2^2\alpha_3^2 + \alpha_3^2\alpha_1^2) + K_{c2}(\alpha_1^2\alpha_2^2\alpha_3^2) + \dots \ . \tag{2.5}$$

α_j are the direction cosine of the magnetization with respect to the cubic axes. The anisotropy constants of selected materials are listed in Table 2.1 together with some other material constants.

To get an impression of the influence of the magnetocrystalline anisotropy on the magnetic behavior let us consider a spherical sample of nickel saturated along the hard axis [100]. Figure 2.3(d) depicts the corresponding magnetization curve. If the applied field H is reduced below the anisotropy field of about 23 mT, the magnetization starts to rotate away from the hard axis, either toward the adjacent <110> directions or to one of the four nearest <111> directions. Only if H is decreased below 15 mT the magnetization steadily rotates toward one of the four easy axes in <111> direction with positive components along [100] to minimize the energy. When H is reduced to zero, all moments lie in <111> directions. This leads to a remanent magnetization of about $1/\sqrt{3}$ of the saturation magnetization M_s [O'H00].

All anisotropy contributions mentioned so far can somehow depend on **magnetoelastic effects** which are negligible in most cases when it comes to domain theory. In cubic crystals such as nickel one of them, namely magnetostriction, can play a role [Lee71]. Magnetostriction means the deformation of a ferromagnet during the magnetization process [Hor71]. It is related to the magnetocrystalline anisotropy since it also originates from spin-orbit interactions. The inverse magnetostrictive effect gives rise to a stress sensibility of magnetic materials that can influence the

Material	Co	Ni	Fe	$Ni_{80}Fe_{20}$	Fe_3O_4
Structure	hcp	fcc	bcc	fcc	spinel
Exchange stiffness A (10^{-11}J/m)	1.3	1.0	2.5	1.3	1.0
Saturation magnetization M_s (10^6 A/m)	1.44	0.483	1.71	0.8	0.48
Anisotropy constant K_1 (10^4J/m^3)	41	-0.45	4.8	-0.03	-0.9
Anisotropy constant K_2 (10^4J/m^3)	15	-0.23	-1.0	-	-

Table 2.1: Fundamental magnetic data at room temperature [Sch91, O'H00, Gol03].